Bulletin of the New Zealand Society for Earthquake Engineering, Vol. 59, No. 3, September 2026

EFFECTS OF GROUND IMPROVEMENT ON THE SEISMIC DEMAND ON BUILDINGS

Romain Meite[1], Liam Wotherspoon[2] and Russell A. Green[3]

(Submitted *October 2024*; Reviewed *December 2024*; Accepted *October 2025*)

ABSTRACT

This paper explores the influence of ground improvement on building seismic demands through parametric site response analyses of low-to-mid-rise buildings supported on mat foundations. A set of soil profiles, containing liquefiable strata, and two building archetypes are analysed using two-dimensional finite element models, both with and without improved zones underneath the buildings. The densification/stiffness of the improved zone and the depth of the improvement is varied as part of the parametric study. The seismic demand on the buildings and foundations for the unimproved and improved sites is assessed. The results show that ground improvement effectively reduces foundation displacements but often increases base shear and inter-storey drift demands. Under total stress conditions, amplified structural seismic demands show a good correlation with increases in shear-wave velocity of the improved ground. However, when liquefiable soil behaviour is modelled, the ratio of the depth of improvement to the depth of the liquefiable stratum ($Z_i/Z_{soft,liq}$) is a more reliable predictor of seismic demands. When $Z_i/Z_{soft,liq} = 0.50$, foundation subsidence relative to the adjacent unimproved ground is limited to less than 50 mm in most cases, and rocking drift remains below 0.5%, provided that bearing pressures do not exceed 80 kPa. This improved depth ratio is identified as a good threshold for limiting the potential for damage. However, beyond this threshold, the ability of the building to sustain repairable damage after an ULS earthquake relies on its capacity to accommodate increased flexural drift caused by soil–foundation–structure interaction effects. The trends identified in this study offer valuable insights into how ground improvement influences seismic demand on buildings.

https://doi.org/10.5459/bnzsee.1717

INTRODUCTION AND BACKGROUND

A variety of ground improvement strategies have been developed to mitigate geotechnical related damage during earthquakes. Ground densification is the most common approach employed to improve the seismic performance of loose granular soils supporting shallow foundations, increasing bearing strength and improving liquefaction resistance (Japanese Geotechnical Society [1]). There is a scarcity of case studies quantifying the effects of ground improvement on the performance of buildings during earthquakes (Karimi and Dashti [2], Olarte et al. [3]). Limited observations from past earthquakes indicate that buildings founded on improved soils undergo less damage than those located in unimproved sites (Ohsaki [4], Mitchell and Wentz [5], Hausler and Koelling [6], Wotherspoon et al. [7]). The reported cases of damage to improved sites generally stem from an insufficient spatial extent of the ground improvement to prevent excessive settlements resulting from the unimproved soil layers that underlie the improved zone. Therefore, experimental testing and numerical analyses are valuable tools that can be used to gain insights into the seismic interactions between the densified soil-foundation systems and the overlying buildings.

Elgamal et al. [8], among others (Liu and Dobry [9], Karamitros et al. [10], Bray and Macedo [11]) showed how a well-calibrated, fluid-solid coupled finite element model can accurately capture liquefaction-induced settlements of shallow foundations resting on a densified crust. Karimi and Dashti [2] performed a series of centrifuge tests and numerical simulations and found that ground densification reduces foundation subsidence but can result in an increase in foundation accelerations and lateral building displacement. Likewise, Olarte et al. [3] used centrifuge tests to compare the seismic performance of 3 and 9-storey steel frames founded on liquefiable soils, with and without ground densification. The results pointed to the importance of the seismic interactions between the densified soil-foundation system and the overlying structure, which can result in higher ductility demands in buildings. Shahir et al. [12], Bray and Macedo [11], and more recently Hwang et al. [13] performed parametric site response analyses of the entire soil-foundation-structure system to derive procedures for estimating liquefaction-induced settlements of sand with various relative densities beneath shallow foundations. While the ability of ground improvement to reduce the seismic displacements of foundations has been widely evaluated in recent decades, the influence on structural response parameters, such as inter-storey drifts and base shear, has received little attention. The need to adopt a holistic strategy for the design of ground improvement is acknowledged in guidelines, in which an iterative process is warranted between geotechnical and structural engineers (NZGS and MBIE [14]). However, a certain number of practical issues need to be addressed to enhance the incorporation of the entire soil-foundation-structure system within a unified framework suitable for a performance based-design approach (Kramer [15]).

Parametric site response analyses are performed in this study to evaluate how the seismic demands of low-to-mid-rise buildings change with the extent of ground improvement considered below a mat foundation. Two-dimensional (2-D) finite element models of soil-foundation-structure systems are implemented using constitutive soil models for total and effective stress conditions. A set of soil profiles representative of the near surface geology of Christchurch are modified by varying the

[1] *Corresponding Author, Lecturer, University of Auckland, Auckland, rmei205@aucklanduni.ac.nz*
[2] *Professor, University of Auckland, Auckland, l.wotherspoon@auckland.ac.nz (Fellow)*
[3] *Professor, Virginia Tech, Blacksburg (USA), rugreen@vt.edu*

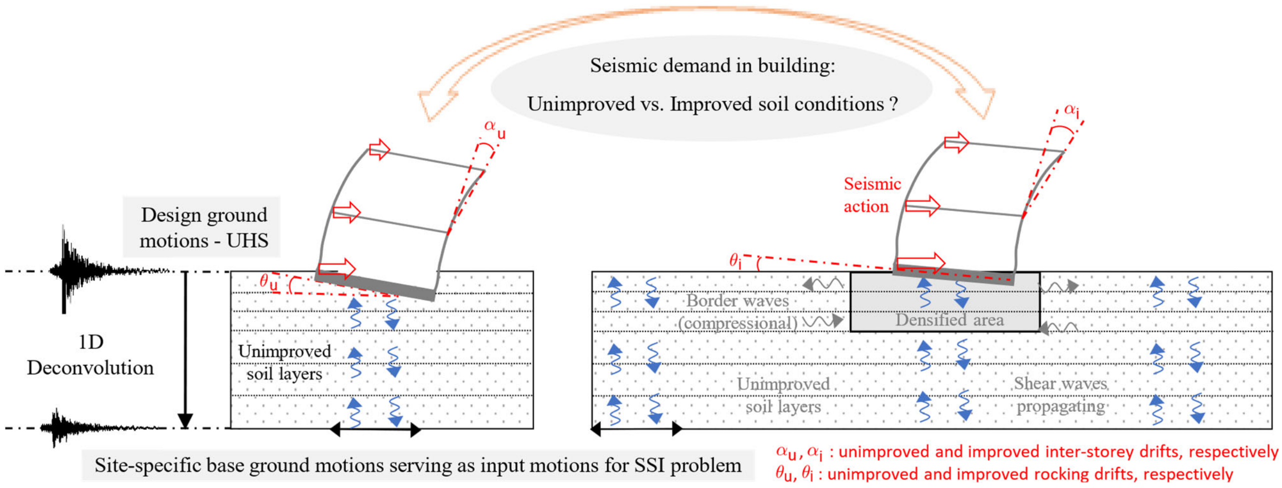

Figure 1: Overview of site response analyses implemented to compare soil-foundation-structure responses with and without ground improvement.

degree of ground densification and depth of improvement. A specific engineering routine is employed to perform hazard-consistent site response analysis for soil foundation-structure interaction (SFSI) problems. In this procedure, which is portrayed in Figure 1, the simulated ground motions at the free field are compatible with the design spectrum provided in standards (i.e., the NZS 1170.5 standard [16]).

The rocking drift arising from the rotation of the foundation, inter-storey drift, and base shear transmitted to the structures are computed for different improved soil conditions. The seismic response factors for various measures (e.g., settlement, drift, base shear), which are defined in the following as the ratio between the improved and unimproved soil model predictions, are examined when increasing the soil relative density, small-strain shear wave velocity (V_S), and depth of improvement. The seismic response of buildings on liquefiable sites, across a range of improved depths, is classified into three levels of seismic demand by comparing the post-shaking engineering demand parameters (EDPs) with the design code limits intended to prevent severe damage.

GEOTECHNICAL CONDITIONS

Representative Soil Profiles for Christchurch

The shallow geology of Christchurch, located in the Canterbury Plains region of New Zealand, consists of recent alluvial soils varying from 10 m thick at the western edge of the city to about 40 m toward the eastern coastline. These shallow soils comprise multiple layers of loose to medium-dense sand, gravel, non-plastic silt, and mixed soils, with substantial variability both vertically and horizontally. The shallow deposits overlie the Riccarton Gravel, which is the uppermost strata of a complex sequence of stiff gravel formations, between 300 m and 500 m thick, interbedded with sand, silt, clay, and peat (Brown and Weeber [17], Cubrinovski et al. [18]).

A set of five soil profiles representative of the near-surface V_S of Christchurch are developed, up to 50 m in depth, and used as a baseline for unimproved site response predictions. It is emphasised that the geotechnical profiles implemented in this study are a simplification of the in situ subsurface conditions of Christchurch. A dry sand deposit is first modelled using total stress analyses, consistent with a profile with a deep aquifer. However, for profiles with a shallower ground water table, effective stress analyses are performed using a water table depth of 1.25 m, which is consistent with values commonly reported in the central business district (CBD) of Christchurch [17,18]. Figure 2 depicts the unimproved V_S profiles implemented for each site, plotted in solid black lines. The depth to the Riccarton Gravel formation varies between 10 and 40 m, with a sharp impedance contrast located at the interface with the overlying sediments. The shear wave velocities for the Riccarton Gravel are approximated using the V_S relationship proposed by Lin et al. [19] for dense gravel and employed in McGann et al. [20] to derive a regional shear wave velocity model for Christchurch. For the sake of simplicity, the overlying loose to medium dense sand layers, whose thicknesses (H_{soft}) range from 10 to 22.5 m across the sites, are assumed to consist of fine, uniform, and clean sands with relative densities (D_R) between 30% and 50%. The sand properties implemented in this study are similar to that of the Nevada Sand as defined by Karimi and Dashti [2]. Table 1 summarises the soil properties employed for the unimproved sites, including the time-averaged V_S over depths of 15 m ($V_{S,15}$) and 30 m ($V_{S,30}$). These values are within the mean and ± one standard deviation of the V_S model for Christchurch defined in McGann et al. (2017), which was centred around $V_{S,15}$ = 147 m/s and $V_{S,30}$ = 194 m/s in the CBD. The unimproved sites are classified as Site Class D for deep/soft soil profiles per the NZS1170.5 New Zealand loadings standard (NZS1170.5 [16]). Based on the draft Technical Specification (DZ TS1170.5:2024 [21]), the unimproved sites fall into the Site Class VI due to the presence of loose to medium-dense soil layers extending to depths of 10 m or greater. For the design ground motions considered in this study, the factor of safety against liquefaction triggering, evaluated following Idriss and Boulanger [22], ranges from 0.18 to 0.30 within the saturated loose to medium-dense sand layers.

Improved Soil Conditions

The upper layers of the soil profiles are modified to include an improved zone comprising a densified crust underneath the buildings. The thickness of ground improvement is varied for each site so that the ratio between the improved zone thickness (H_i) and the initial thickness of the loose to medium dense sand layers (H_{soft}) spans a range of values: H_i/H_{soft} = {0.25, 0.50, 0.75, 1}. While the recommended lateral extent of ground improvement beyond the edge of the foundation is often taken as half the improved zone thickness H_i (Japanese Geotechnical Society [20]), this assumption may not be practical for deep extents of ground improvement due to the presence of adjacent buildings and high costs. Therefore, the lateral extent beyond the foundation edge considered in this study is fixed to 7.5 m by default, regardless of H_i. Three degrees of ground improvement are considered by increasing D_R, shear stiffness via the parameter V_S, and friction angle, which in turn increases

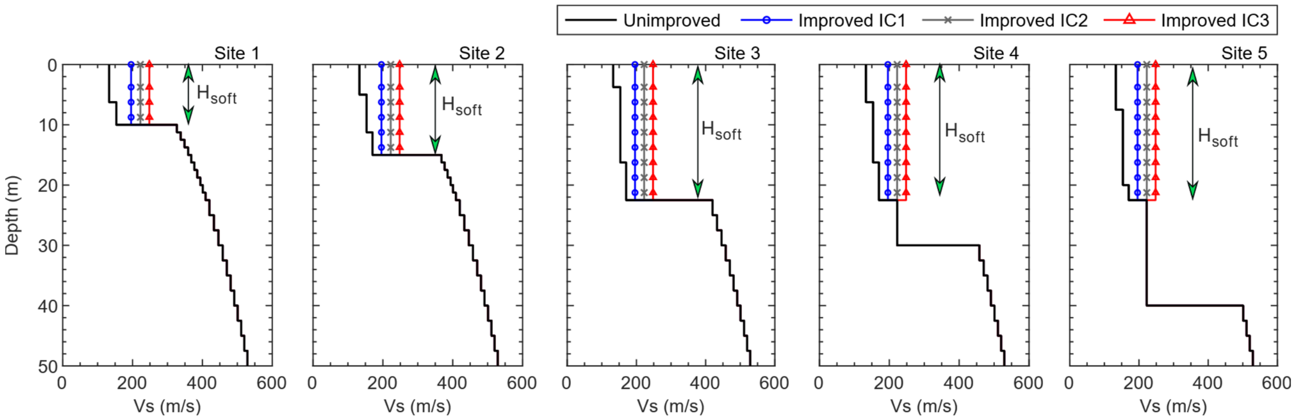

Figure 2: ***V_S profiles employed in this study considering five different subsurface conditions of Christchurch and modified using a range of improved ground conditions IC1, IC2 and IC3 (see Table 2).***

Table 1: Description of the five unimproved site profiles implemented in this study.

Unimproved Sites	H_{soft} (1) (m)	$V_{s,50}$ (m/s)	$V_{s,30}$ (m/s)	$V_{s,15}$ (m/s)	Depth (m)	Soil description	Density (kg/m^3)	ϕ_{peak} (2) (°)
Site 1 (T_0 = 0.65 s)	10	307	245	163	0 -6.25 6.25-10 10-50	Loose sand - D_R = 30% Medium dense sand - D_R = 40% Riccarton Gravel	1950 1960 2000	31 32 36
Site 2 (T_0 = 0.71 s)	15	282	219	148	0-5 5-11.25 11.25-15 15-50	Loose sand - D_R = 30% Medium dense sand - D_R = 40% Medium dense sand - D_R = 50% Riccarton Gravel	1950 1960 1970 2000	31 32 33.5 36
Site 3 (T_0 = 0.82 s)	22.5	245	183	147	0-3.75 3.75-16.25 16.25-22.5 22.5-50	Loose sand - D_R = 30% Medium dense sand - D_R = 40% Medium dense sand - D_R = 50% Riccarton Gravel	1950 1960 1970 2000	31 32 33.5 36
Site 4 (T_0 = 0.89 s)	22.5	224	164	143	0-6.25 6.25-16.25 16.25-22.5 22.5-30 30-50	Loose sand - D_R = 30% Medium dense sand - D_R = 40% Medium dense sand - D_R = 50% Very dense sand - D_R = 90% Riccarton Gravel	1950 1960 1970 2060 2000	31 32 33.5 40 36
Site 5 (T_0 = 1.00 s)	22.5	200	161	142	0-7.5 7.5-20 20-22.5 22.5-40 40-50	Loose sand - D_R = 30% Medium dense sand - D_R = 40% Medium dense sand - D_R = 50% Very dense sand - D_R = 90% Riccarton Gravel	1950 1960 1970 2060 2000	31 32 33.5 40 36

Notes: (1) H_{soft} is the total thickness of loose to medium dense sand layers, which is also the depth to the bottom of the liquefiable layers ($Z_{soft,liq}$);
(2) ϕ_{peak} is the peak friction angle used in OpenSees (octahedral angle).

the soil bearing strength and liquefaction resistance. These improved soil conditions, referred to as IC1, IC2, and IC3, are detailed in Table 2. Figure 2 compared the V_S profiles implemented with and without ground improvement for each site for an improved thickness ratio H_i/H_{soft} = 1. A total of 60 improved soil models (5 sites × 3 degrees of ground improvement × 4 improved thickness ratios) are considered in this study. The additional effects of ground improvement via densification, such as the potential increase in over-consolidation ratio and lateral earth pressures are not considered due to their complexity and the difficulties involved in their quantification.

SOIL-FOUNDATION-STRUCTURE MODEL

In this study, parametric 2-D finite element models are implemented using the open-source platform OpenSees (McKenna [23]), which has long been employed in research to emulate complex behaviours of soils and structures during earthquakes (Elgamal et al. [8]). The numerical modelling approach for the soil-foundation-structure problem is presented in this section.

Constitutive Soil Models

Two constitutive soil models are employed in this study, namely the Pressure Independent Multi-Yield model (PIMY, Yang et al. [24]) for total stress site response analysis when modelling dry sands, and the Pressure Dependent Multi-Yield02 model (PDMY02, Yang et al. [24]) suitable for effective stress conditions with saturated sands susceptible to liquefaction. The deviatoric stress-strain soil response under monotonic or cyclic loading relies on the modified multi-yield surfaces framework (Prevost [25], Parra [26], Yang [27]). In this study, the initial shear stress loading path or backbone curve implemented with the calibrated PDMY02 model parameters, as discussed in the following, is automatically

Table 2: Summary of improved soil conditions considered for parametric site response analyses.

Improved Case	Description	Vs (m/s)	ΔVs*	Thickness (m)	Density (kg/m³)	ϕ_{peak} (°)
IC-1	Dense sand - Dr = 70%	196	50-15%	Variable: H_i/H_{soft} = {0.25, 0.50, 0.75, 1}	2010	36
IC-2	Very dense sand - Dr = 90%	222	65-30 %		2060	40
IC-3	Very dense sand - Dr = 90%	248	90-45%		2060	44

Note: (*) The pair of ΔV_S provided corresponds to the relative change in Vs before and after improvement, calculated at the ground surface and at the depth of 22.5 m.

Table 3: PDMY02 model parameters calibrated for #120 Nevada Sand by Karimi and Dashti (2015a).

Parameters	Nevada Sand					Unit
Relative density, D_R	30	40	50	70	90	%
Saturated unit weight, γ_{sat}	19.13	19.23	19.33	19.72	20.21	kN/m³
Void ratio, e	0.760	0.730	0.700	0.650	0.580	-
Reference pressure, P'_r	101	101	101	101	101	kPa
Pressure dependent coefficient, d	0.5	0.5	0.5	0.5	0.5	-
Shear modulus, G_{ref}	34.5	46.2	57.1	77.1	101.9	MPa
Maximum shear strain, γ_{max}	0.1	0.1	0.1	0.1	0.1	-
Peak friction angle (octahedral), ϕ'_p	31.0	32.0	33.5	36.0	40.0	deg
Phase angle, ϕ_{pt}	31.0	30.0	25.5	26.0	26.5	deg
Contraction parameter 1, *c1*	0.087	0.067	0.05	0.02	0.016	-
Contraction parameter 2, *c2*	5	4.5	4	1.5	1.45	-
Contraction parameter 3, *c3*	0.30	0.27	0.25	0.15	0.14	-
Dilation parameter 1, *d1*	0.01	0.02	0.06	0.15	0.25	-
Dilation parameter 2, *d2*	3.0	3.0	3.0	3.0	3.0	-
Dilation parameter 3, *d3*	0	0	0	0	0	-
Number of yield surfaces	20	20	20	20	20	-
liq1	1	1	1	1	1	-
liq2	0	0	0	0	0	-
Coefficient of permeability, k	7.50x10^{-5}	6.50 x10^{-5}	6.00 x10^{-5}	5.00 x10^{-5}	2.25 x10^{-5}	m/s

generated in OpenSees using a hyperbolic relationship between shear stress and shear strain modified after Kondner and Zelasko [27]. However, for the PIMY model, which does not rely on calibrated parameters, the backbone curve for each soil element is constrained using a set of shear modulus reduction ratios (G/G_{max}) provided in the Darendeli model [28] with strength corrections at large strains (Gingery and Elgamal [29]). For both PIMY and PDMY02 models, the soil damping is implicitly controlled by the shape of the hysteric loops following the original Masing rules. The soil damping ratio at small strains (D_{min}) is set to 2% for all sites and modelled using Rayleigh damping components with two target frequencies, corresponding to the first and fifth site response harmonics calculated for each of the 65 soil profiles considered in this study.

In particular, the PDMY02 model is implemented in conjunction with a fluid-solid coupled plane strain element (QuadUP, Yang et al. [24]), which allows the development of shear-induced contraction and dilation, build-up of pore water pressure, cyclic mobility, and flow liquefaction (Elgamal et al. [11]). The peak excess pore water pressure ratio $r_{u,max}$ predicted using the PDMY02 model is defined as follows:

$$r_{u,max} = \frac{\Delta u_{max}}{\sigma'_{v0}} \tag{1}$$

where Δu_{max} denotes the maximum excess pore water pressure calculated throughout the entire duration of shaking, and σ'_{v0} is the initial effective vertical stress. The PDMY02-calibrated parameters used in this study are summarised in Table 3 for a range of relative densities. The PDMY02 model parameters were calibrated by Karimi and Dashti [2] using undrained cyclic simple shear (CSS) tests on Nevada Sands. The seismic response of structures founded on shallow foundations underlain by liquefiable layers was further verified by comparing the model predictions obtained in OpenSees against centrifuge test results (Karimi and Dashti [2]). The PDMY02-calibrated parameters used in this study are summarised in Table 3 for a range of relative densities.

Archetypes for Moment Resisting Frames

Linear elastic moment resisting frames are employed in this study, i.e., the influence of structural nonlinearities is not included in the model. As such, the elastic base shears calculated are proportional to the elastic forces and bending moments developed in beams and columns. It is noted that the actual response of the frames to intense shaking would likely entail the formation of plastic hinges and that the proportionality between loading and deformation would then differ from that assumed herein. Although the time-history elastic models performed in this study do not fully capture the amplification of building drift ratios due to nonlinear effects, this approach is judged acceptable when assessing the general trends in the seismic demand with and without ground improvement. A damping ratio of 5% is introduced in the finite element models using Rayleigh damping components with two target frequencies, corresponding to the fundamental and third mode of each structure with the details presented as follows.

In this study, 2- and 4-storey reinforced concrete (RC) moment resisting frames archetypes representative of commercial office buildings are modelled using 2-D multiple-degree-of-freedom systems. The structures consist of a three-bay archetype, 27.42 m in total width (B'), with a regular bay spacing in plan so that the torsional effects can be omitted when using a 2-D model. The 2- and 4-storey archetypes implemented in this study are presented in Figure 3. The fundamental periods ($T_{S,1}$) of the 2-

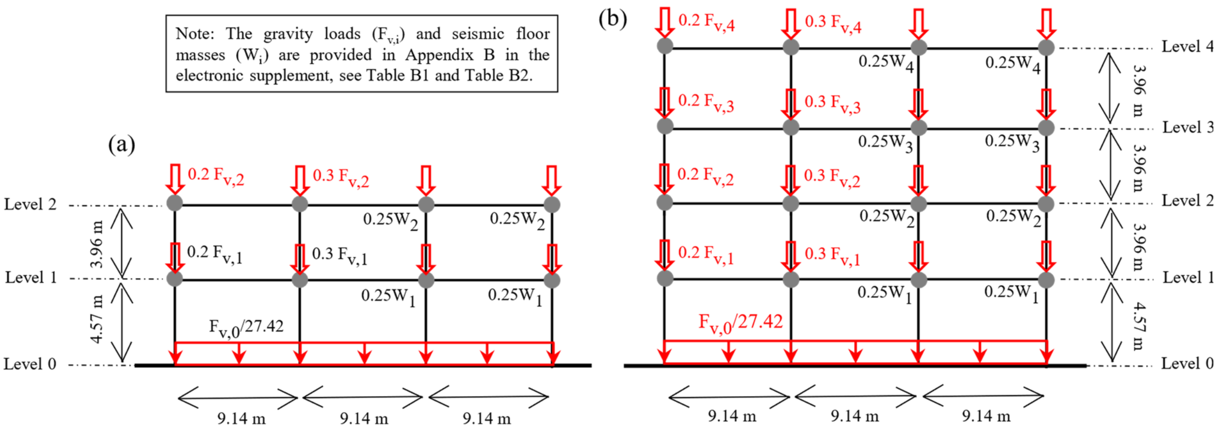

Figure 3: Archetypes for reinforced concrete moment resisting frames: (a) 2-storey building and (b) 4-storey building.

Table 4: Model loading factors applied to the FE model to comply with various areas of active soil pressure below the mat.

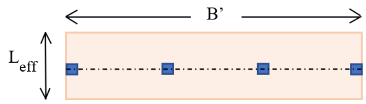

	Site 1	Site 2	Site 3	Site 4	Site 5
Foundation contact pressure targeted in model, q_f (kPa)	40.0	50.0	60.0	70.0	80.0
Model reduction factor $\xi = q_f\ B'/F_v$ for 2-storey frame	0.214	0.267	0.320	0.374	0.427
Model reduction factor $\xi = q_f\ B'/F_v$, for 4-storey frame	0.117	0.146	0.175	0.204	0.233
Effective raft width $L_{eff} = 1/\xi$, for 2-storey frame	4.68	3.75	3.12	2.68	2.34
Effective raft width $L_{eff} = 1/\xi$, for 4-storey frame	8.56	6.85	5.71	4.89	4.28

and 4-storey frames are 0.68 s and 1.17 s, respectively, which are within the range of $T_{S,1}$ expected for similar buildings designed in active seismic regions (Haselton and Deierlein [30], Raghunandan *et al.* [31]). The gravity weight and seismic mass distribution are assigned in the models using nodal forces ($F_{v,i}$) and nodal masses (W_i), respectively. The gravity actions and seismic masses were defined at the Ultimate Limit State (ULS) according to the AS/NZS1170.1 standard [32]. Because it is of primary importance to preserve the dynamic response of the structure to properly capture the SFSI effects, the seismic mass, and the cross-sectional properties of the beams and columns are modified using the approach outlined in the following section. Details about the member's sections and loading distribution per floor are provided in the Appendix in the electronic supplement. When evaluating SFSI effects using a 2-D model, a reduction of structural loads is warranted to provide a soil stress distribution compatible with the volumetric soil response (Popescu and Prevost [34], Adrianopoulos *et al.* [35]). In this study, the foundation bearing pressure (q_f) is adjusted to span a range of values, i.e., q_f = {40, 50, 60, 70, 80} kPa for Sites 1 to 5. This correction is implemented by multiplying the original gravity loads ($F_{v,i}$) and seismic masses (W_i) determined for the 2- and 4-storey interior frames (as shown in Figure 3, with the details provided in Tables A1 and A2 in the Appendix) by a model loading factor ξ defined as follows:

$$\xi = \frac{q_f\ B'}{F_v} \tag{2}$$

where F_v is the total gravity load reaction calculated at ULS for the 2- and 4-storey archetypes (Tables A1 and A2 in the Appendix).

Table 4 summarises the parameters implemented to control the soil stress distribution in the finite element models for each site. The reduction of the foundation bearing pressure via the use of the model loading factor ξ can also be interpreted as varying the width of the active soil pressure zone underneath the shallow foundation (L_{eff}). The gross sections and moments of inertia of beams and columns are reduced by the same factor ξ to ensure that the fundamental periods of the structures remain unchanged. A similar approach was previously implemented by Bray and Macedo [11] to estimate liquefaction-induced building settlement using a 2-D plane strain model.

Parametric 2-D Finite Element Model

2-D site response analyses are performed using 5 sites (Table 1), 4 improved thickness ratios (H_i/H_{soft} = {0.25, 0.50, 0.75, 1}), and 3 degrees of ground improvement (IC1, IC2, and IC3: Table 2), for a total of 60 improved soil models and 5 unimproved soil models. The analyses are performed in total and effective soil stress conditions using the PIMY and PDMY02 constitutive soil models, respectively. The overall soil-foundation-structure system is incorporated into a parametric finite element model, using plane strain elements (Quad and QuadUP, Yang [24]) and flexural beams/columns. The soil profiles, which are modelled as multi-layered soil systems, are subdivided into soil elements so that the maximum mesh thickness in the vertical direction does not exceed $V_S/(8f_{max})$ as commonly recommended in practice (Kuhlemeyer and Lysmer [35]) where f_{max} is the cut-off frequency considered for site response analyses (equal to 15 Hz).

Figure 4 presents the layout of the 2-D finite element model used in this study. The soil system is 230 m in width, 50 m in height, and consists of 4840 quadrilateral elements. The mesh size is refined toward the centre within the footprint of the buildings and at shallow depths to better capture the stress variations underneath the foundation. Periodic boundary conditions are imposed at both lateral ends to simulate an unbounded medium in the far field. The ground motions obtained after deconvolution, as discussed in the following

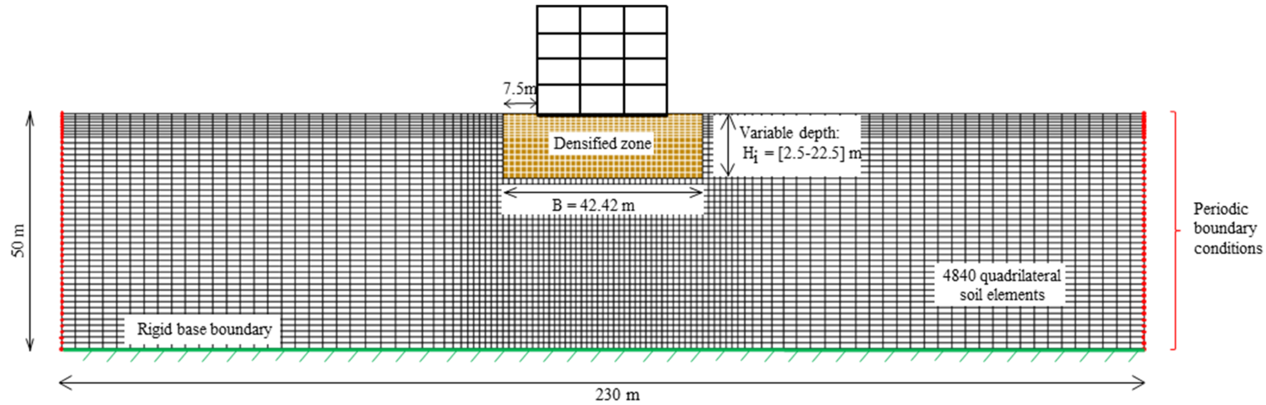

Figure 4: Layout of the 2-D finite element model implemented in OpenSees for parametric site response analyses.

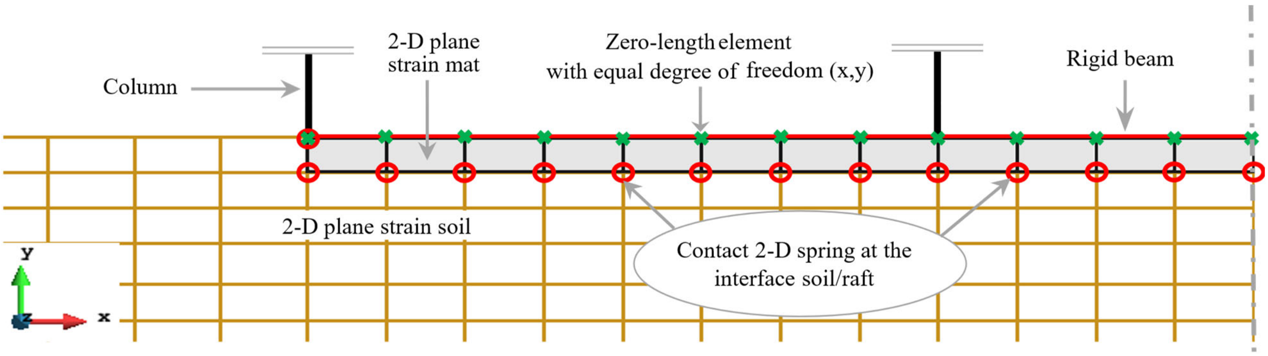

Figure 5: Details of the soil-foundation-structure interface implemented in the finite element model.

section are applied to the rigid base boundary to perform site response analyses.

Details on the interface between soil, mat, and structural elements are shown in Figure 5. An embedded mat, 0.60 m thick for both buildings, is modelled using quadrilateral elements. Zero-length springs constrained with equal degrees of freedom at both ends are employed to connect the mat nodes to the superstructure through a rigid beam connected to the columns. The interface between mat and soil elements is modelled using contact springs (zeroLengthContact2D [24]) assuming a rough contact surface. The advantage of using contact elements is that the rocking drift is consistent with the change in stiffness of the soil elements adjacent to the foundation during shaking. Since the mat foundation is fully embedded, the soil-foundation response is less sensitive to the friction coefficient at the base, and the translational response of the mat follows the ground movement.

INPUT TIME-HISTORY GROUND MOTIONS

In this study, the acceleration design spectrum for Site Class VI in Christchurch, as defined in the draft Technical Specification TS1170.5:2024 [21], is adopted as the target spectrum for the selection of ground motions. The peak ground acceleration (PGA) is equal to 4.12 m/s² (≈ 0.42g), which corresponds to an ultimate limit state (ULS) with an annual probability of exceedance of 1/500 year. A suite of 16 horizontal ground motion acceleration records at the free field from major earthquakes worldwide are selected for their compliance with the seismicity of Christchurch, as well as their goodness of fit to the design spectrum. The motions include two records from the New Zealand GeoNet database compiled by GNS Science [36] and 14 records from the Pacific Earthquake Engineering Research Center database (Ancheta et al. [37]). In this study, a constant scaling factor is applied to the ground motion records to ensure that the mean pseudo-spectral accelerations (PSAs) of selected ground motions envelope the design spectrum over the entire range of oscillator periods. The characteristics of the selected motions as well as their scaling factors are provided in Table 5. The PSAs of each record after scaling and the geometric mean of the scaled records are compared to the design spectrum in Figure 6.

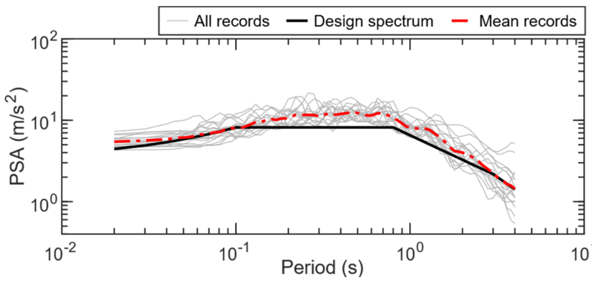

Figure 6: Comparison of the design spectrum at the ground surface and the PSAs of selected ground motions obtained after scaling and before deconvolution.

Previous studies performed by Markham et al. [38], and subsequently by Luque and Bray [39], have shown that the top of the deep Riccarton Gravel formation underlying the upper portion of the soil profiles can be used as a suitable reference horizon to deconvolve ground motions from the Canterbury earthquake sequence and predict SFSI effects on buildings. In this study, the scaled surface ground motions are deconvolved to a rigid base condition at a 50-m depth (i.e., within the Riccarton Gravel) for each of the five unimproved soil profiles (Table 1). The resulting "within-rock" motions from this deconvolution are subsequently applied as input excitations at the base of the 2-D finite element model (Figure 4) to perform site response analyses. The deconvolution of ground motions is performed using one-dimensional visco-elastic transfer functions that relate the surface-to-base ground motion

Table 5: Characteristics of ground motions selected to comply with the design spectrum at the ground surface.

Database	Identifier	M_w	Rrup (km)	PGA (g)	$V_{S,30}$ (m/s)	T_p (s)	AI (m/s)	CAV (m/s)	$D_{5\text{-}95}$ (s)	Scaling Factor
GeoNet	20100903_163541_HORC.S72E	7.08	0.8	0.44	270	0.26	3.18	14.52	8.0	1.33
GeoNet	20100903_163541_ROLC.S61W	7.08	2.1	0.34	210	0.74	1.62	11.58	10.8	2.04
NGA- West2	RSN1082_NORTHR_RO3090	6.69	10.0	0.45	321	0.16	1.46	9.83	16.7	1.54
NGA- West2	RSN1116_KOBE_SHI000	6.90	19.1	0.22	256	0.66	0.83	7.27	10.4	2.16
NGA- West2	RSN1158_KOCAELI_DZC270	7.51	15.4	0.36	282	0.28	1.33	8.08	10.9	1.40
NGA- West2	RSN1495_CHICHI_TCU055-E	7.62	6.3	0.24	359	0.48	1.71	15.35	24.1	2.27
NGA- West2	RSN165_IMPVALL.H_H-CHI282	6.53	7.3	0.25	242	0.68	1.19	11.89	24.0	2.10
NGA- West2	RSN266_VICT_CHI102	6.33	19.0	0.15	242	0.62	0.36	5.01	16.4	3.21
NGA- West2	RSN4853_CHUETSU_65019NS	6.80	27.9	0.21	295	0.80	0.82	10.33	26.5	2.39
NGA- West2	RSN4860_CHUETSU_65033NS	6.80	23.2	0.32	278	0.22	2.03	14.00	19.6	1.76
NGA- West2	RSN5774_IWATE_54008EW	6.90	29.4	0.12	276	0.52	0.71	9.45	25.2	3.46
NGA- West2	RSN582_SMART1.45_45O08EW	7.30	54.8	0.14	357	0.42	0.43	8.41	34.2	3.45
NGA- West2	RSN6_IMPVALL.I_I-ELC270	6.95	6.1	0.21	213	0.58	1.17	12.52	24.1	2.27
NGA- West2	RSN776_LOMAP_HSP090	6.93	27.9	0.18	282	0.52	0.79	10.70	28.8	2.45
NGA- West2	RSN784_LOMAP_TIB290	6.93	72.2	0.25	306	0.32	0.66	6.82	12.6	2.72
NGA- West2	RSN988_NORTHR_CCN360	6.69	23.4	0.22	278	0.24	0.75	8.17	13.6	2.73

Annotations: M_w: moment magnitude; R_{rup}: source-to-site distance; PGA: peak ground acceleration; $V_{S,30}$: time-averaged shear-wave velocity over a depth of 30 m at the station; T_p: predominant period; AI: Arias Intensity; CAV: cumulative absolute velocity; $D_{5\text{-}95}$: significant duration.

amplitudes through a spectral decomposition of site response harmonics. In this study, a recently developed frequency-dependent equivalent linear (FDEL) method (Meite et al. [40]) is employed so that the FDEL model predictions correlate well with the nonlinear model implemented for total stress site response analysis. As such, the ground motion accelerations simulated outside of the improved zone are compatible with the design spectrum and the effects of ground improvement on the seismic demand of buildings are readily quantified by comparing the predictions between improved and unimproved soil models (Figure 1).

ENGINEERING DEMAND PARAMETERS

The engineering demand parameters (EDPs) are assessed in terms of foundation and building responses, both with and without the development of excess pore water pressure in the soil profile (i.e., using total stress and effective stress analyses). Among these EDPs, settlement plays an important role in evaluating the performance of shallow-founded buildings on liquefiable soils. Total settlement is typically conceptualized as the sum of three components: (1) shear-induced settlement beneath the foundation, (2) post-liquefaction volumetric reconsolidation settlement, and (3) ejecta-induced settlement. Karimi and Dashti [2] demonstrated that numerical simulations using the calibrated PDMY02 soil model parameters (Table 3) can effectively reproduce shear-induced settlements and building tilts under dynamic loading with reasonable accuracy. Similarly, Bray and Macedo [11] employed a two-dimensional plane strain model to assess liquefaction-induced settlements beneath buildings. Their findings indicated that although both shear-induced and volumetric reconsolidation settlements may develop during strong shaking, foundation settlement is primarily governed by shear deformation. It is important to note that numerical models do not simulate surface deformation caused by ejecta during shaking, which can be significant in loose, clean sand deposits. In the present study, it is assumed that the improved crust layer mitigates upward seepage of pore water from underlying liquefiable layers, thereby reducing the potential for ejecta manifestation. In addition to settlement, this study also evaluates the influence of ground improvement on foundation rocking and lateral force responses, which are critical design parameters in design because they govern structural stability, damage potential, and serviceability under seismic loading. Excessive rocking can lead to foundation uplift or loss of contact, while large lateral forces can induce significant inter-storey drift and plastic deformation in structural elements. As such, the rocking drift ratio resulting from foundation rotation is calculated directly from raft displacements, assuming the foundation behaves as a rigid body. The elastic base shear developed in the overlying structures is obtained from time-history analyses, and the peak value is normalised by the building weight to determine the base shear ratio. The inter-storey drift, which represents structural distortion, is subsequently obtained by subtracting the contribution of rigid body rocking from the total relative displacement between adjacent storeys. Given that linear elastic moment-resisting frames are used in this study, inter-storey drift ratios from the time-history analyses are multiplied by a drift modification factor (k_{dm}) of 1.25 [16].

SEISMIC DEMAND CRITERIA

The EDPs predicted using numerical simulations are categorized into three levels of seismic demand: “low-to-moderate”, “high”, and “extreme”. The threshold criteria delineating these categories are presented in Table 6. These thresholds are informed by performance-based seismic assessment principles consistent with the NEHRP Guidelines for the Seismic Rehabilitation of Buildings (FEMA 273 [41]), as well as empirical observations from the Canterbury earthquake sequence (2010–2011) in Christchurch [42]. As such:

- A "low-to-moderate" seismic demand indicates that EDP values remain well below the ULS design criteria. Within this range, buildings are expected to experience little to no structural damage, and any liquefaction-induced effects are likely to be minor. Total foundation subsidence, measured relative to the adjacent free field settlement at a lateral offset of approximately B/4 from the building corresponding to the edge of the improved zone, remains below 50 mm, with rocking ratios under 0.1%. This level aligns with FEMA's Immediate Occupancy objective and is considered "readily repairable" per the Canterbury Guidance on House Repairs [43].
- A "high" seismic demand indicates EDP values approaching but not exceeding ULS thresholds. At this stage, structural components may exhibit nonlinear behavior, such as the formation of plastic hinges, though global stability is maintained. Shear connections remain intact, and moderate damage may occur. Van Ballegooy et al. [42] reported that in Christchurch, moderate ejecta and noticeable but repairable floor deformations were common at this level. Total absolute settlements in this range typically span 50–100 mm, and remedial measures such as re-levelling of slabs or repositioning of floor systems may be required. Rocking ratios fall between 0.1% and 0.5%, consistent with FEMA's "Life Safety" performance level [41], as well post-earthquake observations on foundation damage on residential dwellings in Christchurch [42]

Table 6: Classification of seismic demand criteria for buildings.

Seismic demand level	Foundation Settlement	Rocking of foundation	Inter-storey Drift
Low to Moderate	< 50 mm	< 0.1%	< 0.7%
High	50-100 mm	0.1-0.5%	0.7-2%
Extreme	> 100 mm	> 0.5%	> 2%

An "extreme" seismic demand indicates that EDPs exceed ULS design criteria, posing a risk of significant structural damage or partial collapse. Inter-storey drifts exceeding 2% may result in compromised lateral-load-resisting systems, especially where deformation capacity is limited. This level of demand is typically associated with liquefaction-induced settlements exceeding 100 mm and/or foundation rocking ratios above 0.5%. In Christchurch, this corresponded to areas within the residential Red Zone, where Van Ballegooy et al. [42] observed major foundation deformation, extensive liquefaction ejecta, and ground subsidence that rendered buildings irreparable. At this stage, foundation systems are likely to be non-repairable, and demolition may be required. These conditions align with FEMA's "Collapse Prevention" performance level, emphasizing life safety over structural integrity.

TOTAL STRESS SITE RESPONSE ANALYSIS RESULTS

In this section, the seismic responses of the 2- and 4-storey RC frames founded on the improved soil models are examined using total soil stress analyses (PIMY model), appropriate for sites with a deep ground water table. The general trends of the seismic response factors for various measures (e.g., settlement, rocking drift, inter-storey drift, base shear) are discussed in terms of geometric mean and median responses calculated across all sites (×5) and ground motions (×16) for a given improved soil condition.

Effect of Improved Soils on Foundation Response

The influence of ground improvement on the seismic performance is evaluated in terms of foundation displacements for the 2- and 4-storey frames. The median permanent settlements calculated at the end of excitation at the centre of the foundation for the improved soil models (s_i) are compared to the unimproved soil model (s_u) in Figure 7. The settlements predicted when using the unimproved soil models (s_u) increase from Sites 1 to 5 with values between 3.5 and 17 cm (Figure 7a), which is consistent with the foundation bearing pressure applied for each site (Table 4). As expected, the densification and stiffening of bearing soils reduces s_i compared to s_u. However, the extent of settlement reduction is marginal when increasing the degree of ground improvement from IC1 to IC3. The settlement factors s_i/s_u decrease as the improved thickness ratio H_i/H_{soft} increases, with a median s_i/s_u being between 0.78 and 0.54 as H_i/H_{soft} ranges from 0.25 to 1 (Figure 7b).

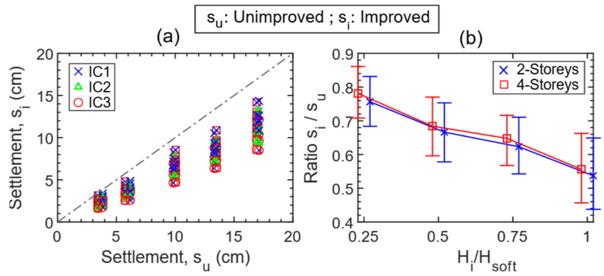

Figure 7: (a) Median settlement predictions in improved soil models (s_i) plotted against unimproved soil models (s_u); (b) median factor s_i/s_u and its 16th-84th percentile intervals plotted against H_i/H_{soft}.

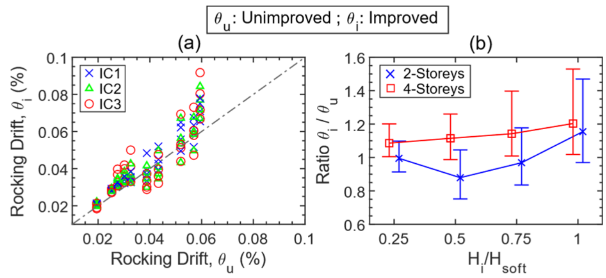

Figure 8: (a) Median rocking drift predictions in improved soil models (θ_i) plotted against unimproved soil models (θ_u); (b) median factor θ_i/θ_u and its 16th-84th percentile intervals plotted against H_i/H_{soft}.

The median rocking drifts obtained for 16 motions and 5 sites for each the 60 improved soil models (θ_i) are plotted in Figure 8 and compared to the unimproved soil model predictions (θ_u). The rocking drift was computed as the ratio between the peak transient differential settlement and the foundation length (27.42 m), which corresponds to the maximum rotation of the foundation during excitation. The unimproved rocking drifts are between 0.02 and 0.06% (Figure 8a). The rocking drift ratios at improved sites exhibit a highly variable trend, with some cases showing increases and others decreases relative to the unimproved conditions. There are minimal differences in the rocking drift ratios across the improved soil conditions (IC1, IC2, and IC3). Instead, the rocking drift response is primarily influenced by the dynamic characteristics of the structures and the SFSI effects. Overall, the rocking drifts developed in the 4-storey frame are amplified across all improved soil models. In this case, the median ratio between the improved and unimproved rocking drifts, θ_i/θ_u, tends to linearly increase with H_i/H_{soft} (Figure 8b), with a median factor $\theta_i/\theta_u \approx 1.2$ when $H_i/H_{soft} = 1$.

In contrast, the rocking drift developed in the 2-storey frame is generally reduced when soft soil layers remain underneath the densified crust such as $H_i/H_{soft} \leq 0.75$, with a median factor θ_i/θ_u comprised between 0.85 and 1.0. The discrepancy of predictions between the 2- and 4-storey models, which were implemented to produce the same foundation contact pressure q_f under gravity loads (Table 4), suggests that the effects of ground improvement on foundation displacements are noticeably affected by the dynamic response characteristics of these structures.

Effect of Improved Soils on Structural Response

The median inter-storey drift (peak transient response) for each improved soil model (α_i) is compared to the unimproved soil model (α_u) in Figure 9. The inter-storey drifts obtained for all improved cases range approximately between 0.7-1.1% for the 2-storey frame, and between 1.3-2.9% for the 4-storey frame, with higher drift ratios corresponding to greater degrees of improvement from IC1 to IC3 (Figure 9a). It should be noted that the inter-storey drift limit recommended for design is 2.5% per the NZS 1170.5 standard [16]. This drift limit could be greatly exceeded when allowing plastic hinges to develop in structural members. Given the relatively low rocking drifts computed previously, the inter-storey drifts are largely dominated by column flexural drifts. For the 2-storey frame, the presence of a densified crust generally yields a slightly higher amplification of the inter-storey drifts compared to the 4-storey frame response, with a median factor α_i/α_u increasing with the improved zone thicknesses; as shown in Figure 9b $1.15 < \alpha_i/\alpha_u < 1.25$. However, for the 4-storey frame, the median inter-storey drift factor α_i/α_u fluctuates around 1.15 for all range of H_i/H_{soft} ratios.

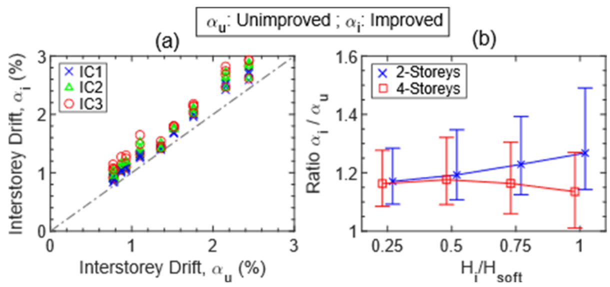

Figure 9: Median inter-storey drift predictions in improved soil models (α_i) plotted against unimproved soil models (α_u); (b) median factor α_i/α_u and its 16th-84th percentile intervals plotted against H_i/H_{soft}.

Figure 10 depicts the median base shear for each improved soil model (F_i) compared to the unimproved soil model (F_u), with F_i and F_u computed as the ratio between the base shear and the gravity weight of the structure (F_v). The normalised base shear obtained increases for all improved soil conditions for both 2- and 4-storey frames, with F_i being between 0.35 and 0.80 (Figure 10a). The results show a noticeable increase in base shear as the improved soil becomes stiffer and denser (IC1, IC2, and IC3). The variations of amplification factors F_i/F_u (Figure 10b) as a function of H_i/H_{soft} are consistent with previous observations of inter-storey drifts for both buildings. This result is expected given that the structures were modelled as linear elastic frames. It is noted that for deep ground improvement, with $H_i/H_{soft} > 0.50$, the base shear factors F_i/F_u calculated using the 2-storey frame are slightly greater than the 4-storey model predictions. These disparities are consistent with the effects of SFSI on floor spectral accelerations discussed previously. The amplification of the seismic demand of improved sites is exacerbated depending on the building's fundamental period ($T_{S,1}$) in relation to the site period. As such, when the overlying structure exhibits a rigid behaviour such as the 2-storey frame, with $T_{S,1}$ within the range of the site periods (T_0, see Table 1) before and after ground improvement, SFSI effects can be particularly detrimental for the seismic demand. This is because multiple modes of resonance may occur in the structure as the soil response harmonics are shifted towards lower periods in improved sites (Meite *et al.* [44]).

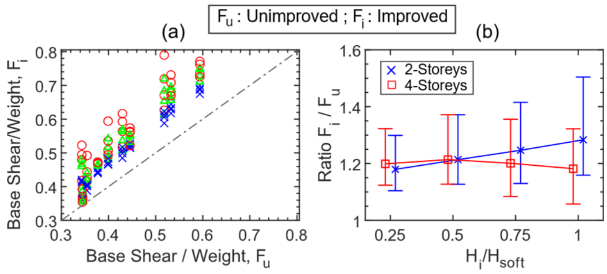

Figure 10: (a) Median base shear predictions in improved soil models (F_i) plotted against unimproved soil models (F_u); (b) median factor F_i/F_u and its 16th-84th percentile intervals plotted against H_i/H_{soft}.

EFFECTIVE STRESS SITE RESPONSE ANALYSIS RESULTS

The effects of extent of ground improvement on the entire soil-foundation-structure response are evaluated in effective soil stress conditions (PDMY02 model) in this section. Liquefaction was triggered, either partially or fully, in all unimproved, saturated loose to medium-dense sand layers across all sites and simulated ground motions. In contrast, all improved soil conditions effectively prevented the buildup of excess pore water pressure to levels approaching liquefaction (i.e., a pore pressure ratio near unity) within the treated zones. The terminology used previously is retained in this section, with the exception that the improved thickness ratio H_i/H_{soft} is replaced by $Z_i/Z_{soft,liq}$, which represents the ratio of the depth of improvement (Z_i) to the depth of the liquefiable stratum ($Z_{soft,liq}$), herein with $Z_{soft,liq} = H_{soft}$.

Effect of Improved Soils on Foundation Response

The effects of ground improvement on the seismic displacements of the mat foundation are evaluated for the 2- and 4-storey frames. Figure 11a presents the median absolute settlement (end of excitation) calculated at the centre of the foundation for each improved soil model as compared to the unimproved soil model ($Z_i/Z_{soft,liq} = 0$). The median absolute values of unimproved site response settlement vary between 63 and 280 cm (Figure 11a) as the foundation contact pressures q_f increases from Sites 1 to 5 (Table 4) along with $Z_{soft,liq}$. While ground improvement reduces foundation settlements compared to unimproved site conditions, there is no clear correlation between the magnitude of settlement reduction and the level of improvement considered (IC1, IC2, and IC3). These results suggest that liquefaction-induced settlements are not governed solely by the degree of improvement; other parameters play a critical role.

Figure 11b depicts foundation settlements as a function of $Z_i/Z_{soft,liq}$ for both absolute settlements at the foundation centre (left ordinate) and settlements relative to the adjacent free-field ground (right ordinate). By convention, a negative relative settlement indicates that the foundation base lies below the surrounding ground surface, while a positive relative settlement indicates that the foundation subsides less than the free-field soil. The results show that although increasing Z_i significantly reduces settlements across all improved soil models, shallow ground improvements, with $Z_i/Z_{soft,liq} < 0.5$, still result in absolute settlements exceeding 50 cm. In contrast, relative foundation settlements indicate that an improvement depth ratio of $Z_i/Z_{soft,liq} > 0.5$ is generally sufficient to keep the foundation elevation above the surrounding free-field ground (i.e., positive relative settlement) in most cases. This occurs because shear-induced settlements beneath the centre of the mat foundation are offset by substantial volumetric reconsolidation settlements in the surrounding ground. Consequently, the need for foundation re-levelling after a ULS earthquake is less likely. Notably, this finding indicates that deep densification of the full thickness of liquefiable strata ($Z_i/Z_{soft,liq}$=1), which is often economically impractical, may not be strictly required to prevent major foundation repairs, provided that foundation rocking drifts remain within acceptable limits, as discussed in the following section.

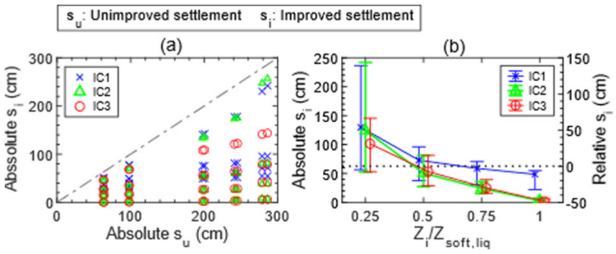

Figure 11: (a) Comparison of median foundation settlement between improved models (s_i) and unimproved models (s_u); (b) median foundation settlement and its 16th-84th percentile intervals plotted against $Z_i/Z_{soft,liq}$, shown for both absolute and relative values.

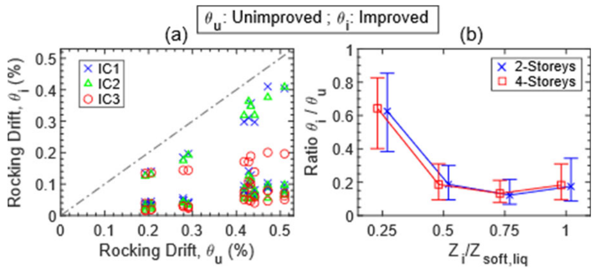

Figure 12: (a) Median rocking drift predictions in improved soil models (θ_i) plotted against unimproved soil models (θ_u); (b) median factor θ_i/θ_u and its 16th-84th percentile intervals plotted against $Z_i/Z_{soft,liq}$

The median rocking drift (peak transient rotation of the foundation) for each improved soil model (θ_i) is compared to the unimproved soil model in Figure 12. The rocking drift values are generally less at improved sites, with greater reductions typically associated with higher degrees of ground improvement from IC1 to IC3 (Figure 12a). The reduction in the rocking drift ratio (θ_i/θ_u) is relatively similar between the 2- and 4-storey frames (Figure 12b). This suggests that the rocking mode effects are mainly controlled by the extreme soil softening that occurs within the underlying liquefiable layers while the structural modes have little influence on this foundation response. In effective soil stress conditions, the increase in $Z_i/Z_{soft,liq}$ does not necessarily increase the rocking drifts as previously observed in the total stress site response analyses. In fact, the θ_i/θ_u factors are less than one for all improved soil model predictions for both 2- and 4-storey frames, with a median θ_i/θ_u factor being substantially reduced down to 0.2 when $Z_i/Z_{soft,liq} \geq 0.50$ (Figure 12b). In this case, the rocking drifts predicted across all improved sites remain within an acceptable range for design ($\theta_i \leq 1/300$, after Bowles 1996 [45]) when $Z_i/Z_{soft,liq} \geq 0.50$.

Effect of Improved Soils on Structural Response

The median inter-storey drift (peak transient response) for each improved soil model is compared to the unimproved soil model in Figure 13. In most cases, the presence of a densified crust underneath the mat increases the inter-storey drifts, along with column flexural drifts. The inter-storey drifts obtained for all improved soil models are comprised between 0.7 and 2.2% for the 2- and 4-storey frames (Figure 13a). Although the relative effect of the degree of ground improvement (IC1, IC2, IC3) on the drift response is not consistently clear, flexural drifts tend to increase with the improved depth ratios $Z_i/Z_{soft,liq}$. A sharp increase is observed for $Z_i/Z_{soft,liq} \geq 0.75$ where the median factors α_i/α_u are between 1.2 and 1.7 (Figure 13b) for both frames.

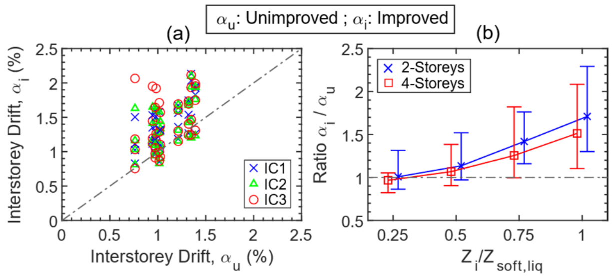

Figure 13: (a) Median inter-storey drift predictions in improved soil models (α_i) plotted against unimproved soil models (α_u); (b) median factor ai/au and its 16th-84th percentile intervals plotted against $Z_i/Z_{soft,liq}$.

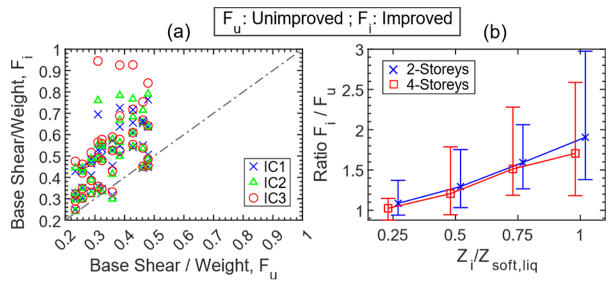

Figure 14: (a) Median base shear predictions in improved soil models (F_i) plotted against unimproved soil models (F_u); (b) median factor Fi/Fu and its 16th-84th percentile intervals plotted against $Z_i/Z_{soft,liq}$.

Figure 14a presents the median base shear for each improved soil model compared to the unimproved soil model. The normalised base shear values obtained using the unimproved soil models range approximately between 0.2 and 0.5 in both 2- and 4-storey frames. A greater scattering is observed across all improved soil model predictions where the normalised base shear raises up to 0.95. The largest base shear amplification generally occurs under the highest degree of ground improvement (IC3). The effects of $Z_i/Z_{soft,liq}$ ratios on the factors F_i/F_u shown in Figure 14b are consistent with previous trends observed for the inter-storey drifts. Likewise, the improvement of the full depth of liquefiable layers ($Z_i/Z_{soft,liq}$=1) tends to almost double the seismic base shear along with forces developed in structural members, with a median factor F_i/F_u between 1.7 and 1.9 for the 4- and 2-storey frames, respectively. The 16th-84th percentile interval of F_i/F_u factor is particularly large for both frames with $Z_i/Z_{soft,liq}$ = 1, which indicates a higher variability in SFSI effects as the thickness of liquefiable soil layers below the densified crust is reduced. The observed variability in base shear is attributed to differences in ground motion intensity measures that are not accounted for by standard spectral acceleration matching with the design spectrum. Shallow liquefiable layers initiate liquefaction earlier due to lower confining pressure and reduced resistance, leading to significant attenuation of seismic energy before it reaches the superstructure across all ground motions. In contrast, deeper liquefiable layers delay the onset of liquefaction, allowing more seismic energy to propagate to the structure depending on the characteristics of the seismic excitation. Preliminary findings also suggest that thicker improved crusts may facilitate faster recovery of shear wave transmission during reconsolidation; however, this warrants further investigation.

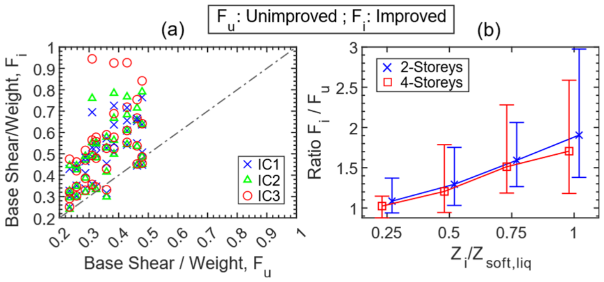

Figure 14: (a) Median base shear predictions in improved soil models (F_i) plotted against unimproved soil models (F_u); (b) median factor Fi/Fu and its 16th-84th percentile intervals plotted against $Z_i/Z_{soft,liq}$.

SEISMIC DEMAND CRITERIA

The effectiveness of ground improvement in mitigating liquefaction-induced damage to buildings is assessed by categorizing the EDPs into three levels of seismic demand based on the criteria outlined in the methodology section (see Table 6). Figure 15 summarises the distribution of seismic demand levels across all effective stress analyses (2080 in total) for various improved depth ratios $Z_i/Z_{soft,liq}$, encompassing five sites, three improved soil conditions (IC1, IC2, IC3), two building archetypes, and 16 ground motions.

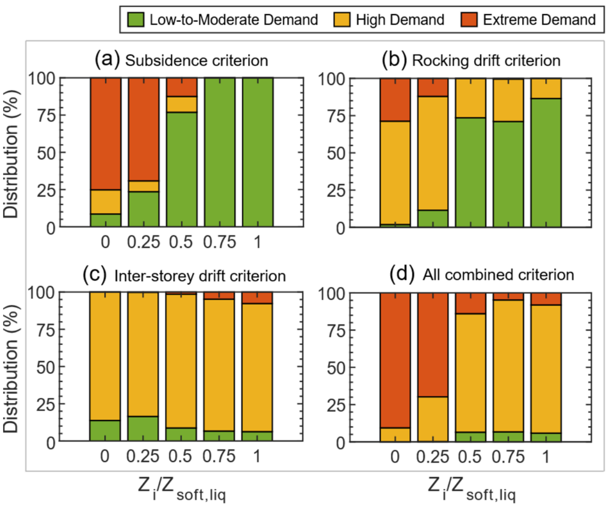

Figure 15: Distribution of seismic demand levels on buildings from all effective stress analyses, plotted against $Z_i/Z_{soft,liq}$, for various EDPs: (a) foundation subsidence, (b) foundation rocking drift, (c) inter-storey drift ratio, and (d) all criteria combined.

When considering foundation subsidence alone (Figure 15a), the data show a marked reduction in the severity of seismic demand when $Z_i/Z_{soft,liq} \geq 0.50$. As such, in over 77% of improved cases with $Z_i/Z_{soft,liq} = 0.50$, foundation subsidence relative to the surrounding free-field ground surface are less than 50 mm, falling within the Low-to-Moderate category. This outcome is attributed to the fact that reconsolidation settlements developed in the unimproved layers at the free field exceed shear-induced settlements simulated at the centre of the improved zone when $Z_i/Z_{soft,liq} \geq 0.50$. A similar trend is observed for the rocking drift ratio (Figure 15b). At shallow improvement depths ($Z_i/Z_{soft,liq} \leq 0.25$), rocking drift ratio is predominantly High (70%) to Extreme (29%). However, when $Z_i/Z_{soft,liq} \geq 0.50$, the seismic demand distribution shifts, with 73.5% of cases classified as Low-to-Moderate and the remainder (26.5%) as High. In contrast, inter-storey drift ratios (Figure 15c) exhibit persistently High seismic demand for approximately 85% of cases, regardless of $Z_i/Z_{soft,liq}$. Furthermore, the proportion of Extreme inter-storey drift demands increases with greater improvement depth, reaching up to 8% at $Z_i/Z_{soft,liq} = 1$. This suggests that while deep ground improvement is effective in reducing foundation-related demands, it may not mitigate structural deformation demands and could increase the potential for more severe demands. When considering the envelope seismic demand across all criteria for each case (Figure 15d), the Extreme demand is below 15% when $Z_i/Z_{soft,liq} = 0.50$. In these cases, most results fall within the High demand category. When $Z_i/Z_{soft,liq} \geq 0.5$, building damage potential is primarily governed by the structure's ability to accommodate higher inter-storey drift demands. Overall, the results presented suggest that improving at least half the depth of the liquefiable soil layer ($Z_i/Z_{soft,liq} \geq 0.50$) is generally sufficient to prevent severe foundation damage. However, increased inter-storey drift may result in significant structural damage if SFSI effects are not properly considered in the design process.

CONCLUSIONS

Results from parametric 2-D site response analyses were presented to evaluate the effects of ground improvement on the elastic seismic demands of low-to-mid-rise reinforced concrete moment resisting frames resting on a mat foundation underlain by a clean sand deposit. The thickness, soil density, and stiffness of the improved zones were all varied relative to the unimproved sites. The general trends in model predictions were derived using 16 ground motions, 5 soil profiles containing liquefiable layers, and 12 extents of ground improvement.

It was found that the reduction of foundation displacements across all cases of ground improvement is accompanied by an increase in base shear and inter-storey drift developed in the structures. For total stress conditions, the amplification factor between improved and unimproved site responses strongly depends on the relative increase in Vs due to improving the ground. However, when considering saturated sand deposits with liquefiable strata, the increase in seismic base shear after ground improvement is not governed by the increase in Vs. In this case, the depth of improvement normalised by the depth of the liquefiable stratum ($Z_i/Z_{soft,liq}$) is a good proxy for predicting the amplification factors for the seismic response measures for the improved sites relative to those for the unimproved sites. There is a substantial increase in the inter-storey drift and base shear when $Z_i/Z_{soft,liq} \geq 0.50$, with a median amplification factor varying from 1.4 (for $Z_i/Z_{soft,liq} = 0.50$) to approximately 2 (for $Z_i/Z_{soft,liq} = 1$). As such, the improvement of the full depth of liquefiable layers can significantly increase the inter-storey drifts and structural forces compared to the unimproved soil model predictions. On the other hand, a densified crust overlying liquefiable layers tends to reduce the seismic demand of buildings despite being less effective in reducing absolute settlements. More specifically, when foundation settlement is evaluated relative to the adjacent free-field ground surface, an improved depth ratio of $Z_i/Z_{soft,liq} = 0.50$ is sufficient to restrict foundation subsidence to less than 50 mm in over 85% of cases, provided that bearing pressures on the raft foundation do not exceed 80 kPa. In addition, the rocking drift of the foundation remains below 0.5% across all improved sites when $Z_i/Z_{soft,liq} \geq$

0.50. This depth ratio is therefore identified as a good threshold for enhancing the seismic performance of buildings on mat foundations. Beyond this threshold, however, the ability of the building to sustain repairable damage following an ULS earthquake relies on its capacity to accommodate the increased flexural drift induced by soil–foundation–structure interaction effects.This paper provides an example of a hazard-consistent site response study that can be performed to better anticipate the effects of ground improvement on the seismic demand of buildings. The effects of ground water table, control ground motion intensities, and structural nonlinearities on the relative amplification of seismic actions have not been investigated in this study and should be evaluated in future work.

ACKNOWLEDGMENTS

The authors acknowledge the financial support of the New Zealand Natural Hazards Commission University Research Programme and QuakeCoRE, a New Zealand Tertiary Education Commission-funded Centre. This is QuakeCoRE publication number 1168. We also wish to acknowledge the use of New Zealand eScience Infrastructure (NeSI) high performance computing facilities, consulting support and/or training services as part of this research. New Zealand's national facilities are provided by NeSI and funded jointly by NeSI's collaborator institutions and through the Ministry of Business, Innovation & Employment's Research Infrastructure programme. URL https://www.nesi.org.nz.

REFERENCES

1 Japanese Geotechnical Society (1998). "*Remedial Measures against Soil Liquefaction from Investigation and Design to Implementation*". Rotterdam: A. A. Balkema.

2 Karimi Z and Dashti S (2016). "Seismic performance of shallow founded structures on liquefiable ground: validation of numerical simulations using centrifuge experiments". *Journal of Geotechnical and Geoenvironmental Engineering*, **142**(6). https://doi.org/10.1061/(ASCE)GT.1943-5606.0001479

3 Olarte J, Dashti S and Liel AB (2018). "Can ground densification improve seismic performance of the soil-foundation-structure system on liquefiable soils*?"* *Earthquake Engineering and Structural Dynamics*, **47**(5): 1193-1211. https://doi.org/10.1002/eqe.3012

4 Ohsaki Y (1970). "Effects of sand compaction on liquefaction during the Tokachioki earthquake". *Soils and Foundations*, **10**(2): 112-128. https://doi.org/10.3208/sandf1960.10.2_112.

5 Mitchell JK and Wentz FJ (1991). "*Performance of improved ground during the Loma Prieta Earthquake*". Report No. UCB/EERC-91/12, Earthquake Engineering Research Center, University of California at Berkeley, Berkeley, CA. https://nehrpsearch.nist.gov/article/PB93-114791/XAB

6 Hausler EA and Koelling M (2004). "Performance of improved ground during the 2001 Nisqually earthquake". *5th International Conference on Case Histories in Geotechnical Engineering*, New York, NY. https://scholarsmine.mst.edu/icchge/5icchge/session03/18.

7 Wotherspoon LM, Orense RP, Jacka M, Green RA, Cox BR and Wood CM (2014). "Seismic performance of improved ground sites during the 2010–2011 Canterbury earthquake sequence". *Earthquake Spectra*, **30**(1): 111-129. https://doi.org/10.1193/082213EQS236M

8 Elgamal A, Lu J and Yang Z (2005). "Liquefaction-induced settlement of shallow foundations and remediation: 3D numerical simulation". *Journal of Earthquake Engineering*, **9**: 17-45. https://doi.org/10.1080/13632460509350578

9 Liu L and Dobry R (1997). "Seismic response of shallow foundation on liquefiable sand". *Journal of Geotechnical and Geoenvironmental Engineering*, **123**(6): 557-567. https://doi.org/10.1061/(ASCE)1090-0241(1997)123:6(557)

10 Karamitros DK, Bouckovalas GD and Chaloulos YK (2013). "Insight into the seismic liquefaction performance of shallow foundations". *Journal of Geotechnical and Geoenvironmental Engineering*, **139**(4): 599-607. https://doi.org/10.1061/(ASCE)GT.1943-5606.000079

11 Bray JD and Macedo J (2017). "6th Ishihara Lecture: Simplified procedure for estimating liquefaction-induced building settlement". *Soil Dynamics and Earthquake Engineering*, **102**: 215-231. https://doi.org/10.1016/j.soildyn.2017.08.026

12 Shahir H, Pak A and Ayoubi P (2016). "A performance-based approach for design of ground densification to mitigate liquefaction". *Soil Dynamics and Earthquake Engineering*, **90**: 381-394. https://doi.org/10.1016/j.soildyn.2016.09.014

13 Hwang YW, Bullock Z, Dashti S and Liel A (2022). "A probabilistic predictive model for foundation settlement on liquefiable soils improved with ground densification". *Journal of Geotechnical and Geoenvironmental Engineering*. https://doi.org/10.1061/(ASCE)GT.1943-5606.0002768

14 NZGS and MBIE (2016). "*Earthquake Geotechnical Engineering Practice in New Zealand – Module 4: Earthquake resistant foundation design. New Zealand*". Geotechnical Society and Ministry of Business Innovation & Employment. https://www.building.govt.nz/building-code-compliance/b-stability/b1-structure/module-4-earthquake-foundation-design

15 Kramer SL (2008). "Performance-based earthquake engineering: Opportunities and implications for geotechnical engineering practice". *Geotechnical Earthquake Engineering and Soil Dynamics,* **IV**: 1-32. https://doi.org/10.1061/40975(318)213

16 Standards New Zealand (2004). "*NZS1170.5: Structural Design Actions. Part 5: Earthquake Actions - New Zealand*". Standards New Zealand, Wellington, 76pp. https://www.standards.govt.nz/sponsored-standards/building-standards/NZS1170-5

17 Brown LJ and Weeber JH (1995). "Geology of Christchurch, New Zealand". *Environmental and Engineering Geoscience*. https://doi.org/10.2113/gseegeosci.I.4.427

18 Cubrinovski M, Bradley B, Wotherspoon L, Green R, Bray J, Wood C, Pender M, Allen J, Bradshaw A, Rix G and Taylor M (2011). "Geotechnical aspects of the 22 February 2011 Christchurch earthquake". *Bulletin of the New Zealand Society for Earthquake Engineering*. **44**(4): 205-226. https://doi.org/10.5459/bnzsee.44.4.205-226

19 Lin YC, Joh SH and Stokoe K (2014). "*Analysis of the UTexas 1 surface wave dataset using the SASW methodology*". in: Geo-Congress Technical Papers, GSP **234**: 830–839. https://doi.org/10.1061/9780784413272.081

20 McGann CR, Bradley BA and Cubrinovski M (2017). "Development of a regional Vs30 model and typical Vs profiles for Christchurch, New Zealand from CPT data and region-specific CPT-Vs correlation". *Soil Dynamics and Earthquake Engineering*, **95**: 48-60. https://doi.org/10.1016/j.soildyn.2017.01.032

21 Standards New Zealand (2025). "*TS 1170.5 Supp 1:2025, New Zealand Technical Specification. Commentary to Structural Design Actions Part 5: Earthquake Actions – New Zealand*". https://www.standards.govt.nz/shop/snz-ts-1170-5-supp-12025

22 Idriss IM and Boulanger RW (2008). "*Liquefaction during Earthquakes*". Earthquake Engineering Research Institute, Oakland, CA.

23 McKenna F (2011). "*OpenSees: A framework for earthquake engineering simulation*". Computing in Science & Engineering, **13**(4): 58-66. http://opensees.berkeley.edu/

24 Yang Z, Lu J and Elgamal A (2008). "*OpenSees soil models and solid-fluid fully coupled elements*". User's Manual. Version 1, 27.

25 Prevost JH (1985). "A simple plasticity theory for frictional cohesionless soils". *Soil Dynamics and Earthquake Engineering*, **4**(1): 9-17. https://doi.org/10.1016/0261-7277(85)90030-0.

26 Parra-Colmenares EJ (1996). "*Numerical modeling of liquefaction and lateral ground deformation including cyclic mobility and dilation response in soil systems*". PhD Dissertation, Department of Civil Engineering, Rensselaer Polytechnic Institute, Troy, NY.

27 Kondner RL and Zelasko JS (1963). "Hyperbolic stress-strain formulation for sands". *2nd Pan American Conference on Soil Mechanics and Foundation Engineering (ISSMGE).* 289–324. https://cir.nii.ac.jp/crid/1572261549806272256

28 Darendeli MB (2001). "*Development of a New Family of Normalized modulus reduction and material damping curves*". PhD Dissertation, Department of Civil Engineering, University of Texas at Austin, TX.

29 Gingery JR and Elgamal A (2013). "*Shear stress-strain curves based on the G/Gmax logic: A procedure for strength compatibility*". IACGE: Challenges and Recent Advances in Geotechnical and Seismic Research and Practices, 721-729. https://doi.org/10.1061/9780784413128.083

30 Haselton CB and Deierlein GG (2007). "*Assessing seismic collapse safety of modern reinforced concrete frame buildings*". PEER Report 2007/08, PEER Center, University of California, Berkeley, CA. http://ir.vnulib.edu.vn/handle/123456789/1719

31 Raghunandan M, Liel AB and Luco N (2015). "Collapse risk of buildings in the Pacific northwest region due to subduction earthquakes". *Earthquake Spectra*, **31**(4): 2087-2115. https://doi.org/10.1193/012114EQS011M

32 AS/NZS 1170.1 (2002). "*Structural Design Actions, Part 1: Permanent, Imposed and Other Actions*". Standards Australia/Standards New Zealand, Wellington, New Zealand.

33 Popescu R and Prevost JH (1995). "Comparison between VELACS numerical 'class A' predictions and centrifuge experimental soil test results". *Soil Dynamics and Earthquake Engineering*, **14**(2): 79-92. https://doi.org/10.1016/0267-7261(94)00038-I

34 Adrianopoulos KI, Papadimitriou AG and Bouckovalas GD (2010). "Bounding surface plasticity model for the seismic liquefaction analysis of geostructures". *Soil Dynamics and Earthquake Engineering*, **30**: 895–911. https://doi.org/10.1016/j.soildyn.2010.04.001

35 Kuhlemeyer RL and Lysmer J (1973). "Finite element method accuracy for wave propagation problems". *Journal of Soil Mechanics and Foundations Division*, **99**(5): 421-427. https://doi.org/10.1061/JSFEAQ.0001885

36 GNS Science, GeoNet. "*Geological Hazard Information for New Zealand*". https://www.geonet.org.nz (Accessed 15 May 2025)

37 Ancheta TD, Darragh RB, Stewart JP, Seyhan E, Silva WJ, Chiou BS, Wooddell KE, Graves RW, Kottke AR and Boore DM (2014). "NGA-West2 Database". *Earthquake Spectra*. https://doi.org/10.1193/070913EQS197M

38 Markham C, Bray JD, Macedo J and Luque R. (2016). "Evaluating nonlinear effective stress site response analyses using records from the Canterbury earthquake sequence". *Soil Dynamics and Earthquake Engineering,* **82**: 84–98. https://doi.org/10.1016/j.soildyn.2015.12.007

39 Luque R and Bray JD (2020). "Dynamic soil-structure interaction analyses of two important structures affected by liquefaction during the Canterbury earthquake sequence". *Soil Dynamics and Earthquake Engineering*, **133**. https://doi.org/10.1016/j.soildyn.2019.106026

40 Meite R, Wotherspoon L, McGann CR, Green RA and Hayden C (2020). "An iterative linear procedure using frequency-dependent soil parameters for site response analyses". *Soil Dynamics and Earthquake Engineering*, **130**. https://doi.org/10.1016/j.soildyn.2019.105973

41 FEMA (1997). "*NEHRP Guidelines for the Seismic Rehabilitation of Buildings*". FEMA 273, 1997 Edition. Federal Emergency Management Agency, Washington, D.C.

42 Van Ballegooy S, Malan P, Lacrosse V, Jacka ME, Cubrinovski M, Bray JD, O'Rourke TD, Crawford SA and Cowan H (2014). "Assessment of liquefaction-induced land damage for residential Christchurch". *Earthquake Spectra*, **30**(1): 31-55 https://doi.org/10.1193/031813EQS070M

43 Department of Building and Housing (2010). "*Guidance on House Repairs and Reconstruction Following the Canterbury Earthquake*". Paper No. 380. Department of Building and Housing, Wellington. ISBN 978-0-478-34376-2.

44 Meite R, Wotherspoon L and Green R (2022). "Influence of extent of remedial ground densification on seismic site effects via 2-D site response analyses". *Soil Dynamics and Earthquake Engineering*, **152**. https://doi.org/10.1016/j.soildyn.2021.107041

45 Bowles JE (1996). "*Foundation Analysis and Design*". 5th Edition, New York: McGraw-Hill Companies, Inc.